Temperature dependence of spin-orbit torques in Cu-Au alloys

Yan Wen,[1] Jun Wu,[2] Peng Li,[1] Qiang Zhang,[1] Yuelei Zhao,[1] Aurelien Manchon,[1,*] John Q. Xiao,[2,†] and Xixiang Zhang[1,‡]
[1]*King Abdullah University of Science and Technology, Physical Science and Engineering Division, Thuwal 23955 6900, Saudi Arabia*
[2]*University of Delaware, Department of Physics and Astronomy, Newark, Delaware 19716, USA*
(Received 16 September 2016; revised manuscript received 1 January 2017; published 6 March 2017)

We investigated current driven spin-orbit torques in $Cu_{40}Au_{60}/Ni_{80}Fe_{20}$/Ti layered structures with in-plane magnetization. We have demonstrated a reliable and convenient method to separate dampinglike torque and fieldlike torque by using the second harmonic technique. It is found that the dampinglike torque and fieldlike torque depend on temperature very differently. Dampinglike torque increases with temperature, while fieldlike torque decreases with temperature, which are different from results obtained previously in other material systems. We observed a nearly linear dependence between the spin Hall angle and longitudinal resistivity, suggesting that skew scattering may be the dominant mechanism of spin-orbit torques.

DOI: 10.1103/PhysRevB.95.104403

I. INTRODUCTION

Bulk materials and/or interfaces with large spin-orbit coupling have attracted significant attention recently, since they can generate substantial spin current or spin accumulation that can be used to manipulate the magnetic moment [1–8]. When spin current is generated by a nonmagnetic (NM) layer via the spin Hall effect (SHE), the accumulated spins can diffuse into the ferromagnetic (FM) layer and interact with the magnetic moment of the FM layer via spin transfer torque. Spin accumulation can also be generated electrically at the NM/FM interface via the Rashba effect [5,9]. It has been theoretically predicted that both the Rashba effect at the NM/FM interface and the SHE in the bulk of the NM layer generate dampinglike torque and fieldlike torque upon magnetization [10]. Some recent theories also suggested that spin swapping can contribute to spin-orbit torque (SOT) [11].

The physics underlying SOT can be investigated when dampinglike torque and fieldlike torque are separated. Recently, second harmonic voltage measurements [12] were used to evaluate the effective field induced by dampinglike torque and fieldlike torque [6,13–18]. This technique has been widely used to characterize SOT in magnetic heterostructures that possess out of plane magnetization and/or have a significant perpendicular magnetic anisotropy. Therefore, a similar electrical measurement technique is needed to characterize the systems with in-plane magnetization [15,17,19,20].

The study of the temperature dependence of SOTs is important because it can provide useful information about the physics and mechanisms of SOTs. An accurate understanding of the physics of SOTs is crucial to the efficient structural design of SOT devices. Qiu *et al.* [21] reported that fieldlike torque decreased linearly with decreasing temperature in Ta/CoFeB/MgO samples, whereas the dampinglike torque mostly remained unaffected. The two different dependences suggest that scattering events involving magnons and phonons play different roles in the two torque components. However, most previous studies focused on Ta [21,22] or Pt based materials in which intrinsic SHE dominates [23,24].

In this paper, we used a technique to characterize SOTs in materials with in-plane magnetization by modifying the technique previously used on materials with perpendicular magnetization. Using this technique, we studied the SOTs in CuAu/NiFe heterostructures as a function of NM layer thickness and temperature. It was found that both fieldlike torque and dampinglike torque increased monotonically with the thickness of the nonmagnetic underlayer, as explained by a simple drift diffusion model [25]. However, the dampinglike torque and the fieldlike torque exhibited different temperature behaviors, suggesting that SOT is driven by extrinsic scattering events in this system.

II. HARMONIC RESPONSE MODEL

It is now well known that an in-plane current flowing through a NM/FM heterostructure with strong spin-orbit coupling can generate two different SOTs: dampinglike torque $\sim\vec{m}\times(\vec{\sigma}\times\vec{m})$ and fieldlike torque $\sim\vec{m}\times\vec{\sigma}$, where $\vec{m}$ is the normalized magnetization vector and $\vec{\sigma}$ is the accumulated spin direction. To calculate the magnetization direction (θ_m,φ_m), we look for the minimum energy states by considering the anisotropy energy and the Zeeman energy [17] (see Appendix). After an alternative current, $i = I\sin(\omega t)$ is injected, and the Hall resistance $R(t)$ oscillates at the same frequency. The Hall voltage $V(t) = R(t)I\sin(\omega t)$, thus, gives information about the current induced fields. It can also be separated into two parts based on their frequency (see Appendix):

$$V_H = [R_P \sin 2\varphi_m \sin\omega t + (\Delta\varphi \cdot 2R_p \cos 2\varphi_m - \Delta\theta \cdot R_A)\sin^2\omega t]I, \quad (1)$$

where R_A and R_P are the coefficients of the anomalous Hall effect (AHE) and the planar Hall effect (PHE), respectively; $\Delta\theta,\Delta\varphi$ is the change in the polar and azimuthal angles of magnetization under current induced fields, θ_m,φ_m are the polar and azimuthal angles of magnetization in sphere coordinates. We define $\theta = 0$ as the direction perpendicular to the film plane, and $\varphi = 0$ is the direction parallel to current. The second

*Aurelien.Manchon@kaust.edu.sa
†jqx@udel.edu
‡xixiang.zhang@kaust.edu.sa

order term can be separated out as

$$V_{2\omega} = \left(-\Delta\varphi \cdot R_p \cos 2\varphi_m + \tfrac{1}{2}\Delta\theta \cdot R_A\right) I. \quad (2)$$

If the external magnetic field applied in the film plane ($\theta_H = \pi/2$) is strong enough to keep the magnetic moment almost in-plane ($\theta_m \cong \pi/2$), we can obtain the following equation

$$V_\omega = R_P \sin 2\varphi \cdot I$$
$$V_{2\omega} = \left(\frac{-H_{\mathrm{FL}} \cos\varphi}{H - H_A} \cdot R_p \cos 2\varphi + \frac{1}{2}\frac{H_{\mathrm{DL}} \cos\varphi}{H_K - H} \cdot R_A\right) I, \quad (3)$$

where H_K and H_A are the effective out of plane and in-plane anisotropy field, respectively. Given the above relations, a larger external field significantly decreases the second order voltage. To overcome this problem, we choose some optimized fields that can both fulfill the approximation requirement and obtain strong and measurable signals. By scanning the angle of the external field in-plane, the effective fields induced by fieldlike torque and dampinglike torque can be obtained.

III. EXPERIMENTAL DETAILS

$Cu_{40}Au_{60}/Ni_{80}Fe_{20}/Ti$ layered structures were fabricated on SiO_2/Si substrates at room temperature using sputtering. Electrical transport properties and magnetic properties of the samples were characterized over a wide temperature ranging from 20 to 300 K under different magnetic fields. The SOTs were measured by the second harmonic Hall voltage method. An ac voltage of 5 V with a frequency of 87.34 Hz was applied using an SR830 lock in amplifier.

IV. RESULTS AND DISCUSSION

Shown in Fig. 1(a) is the schematic of the measurement setup for CuAu (8 nm)/NiFe (1.5 nm)/Ti (1 nm) samples. Figure 1(b) shows the first harmonic voltage V_ω as a function of the azimuthal angle φ, measured under a magnetic field $H = 50$ Oe at different temperatures (20 to 300 K). To obtain the coefficient of the PHE R_P, we fitted the data to $V_\omega = R_P \sin 2\varphi_m \cdot I$. We note that R_P is independent of the field at higher fields and that the data follow $\sin 2\varphi$ dependence very well, indicating that the moment is always along with the

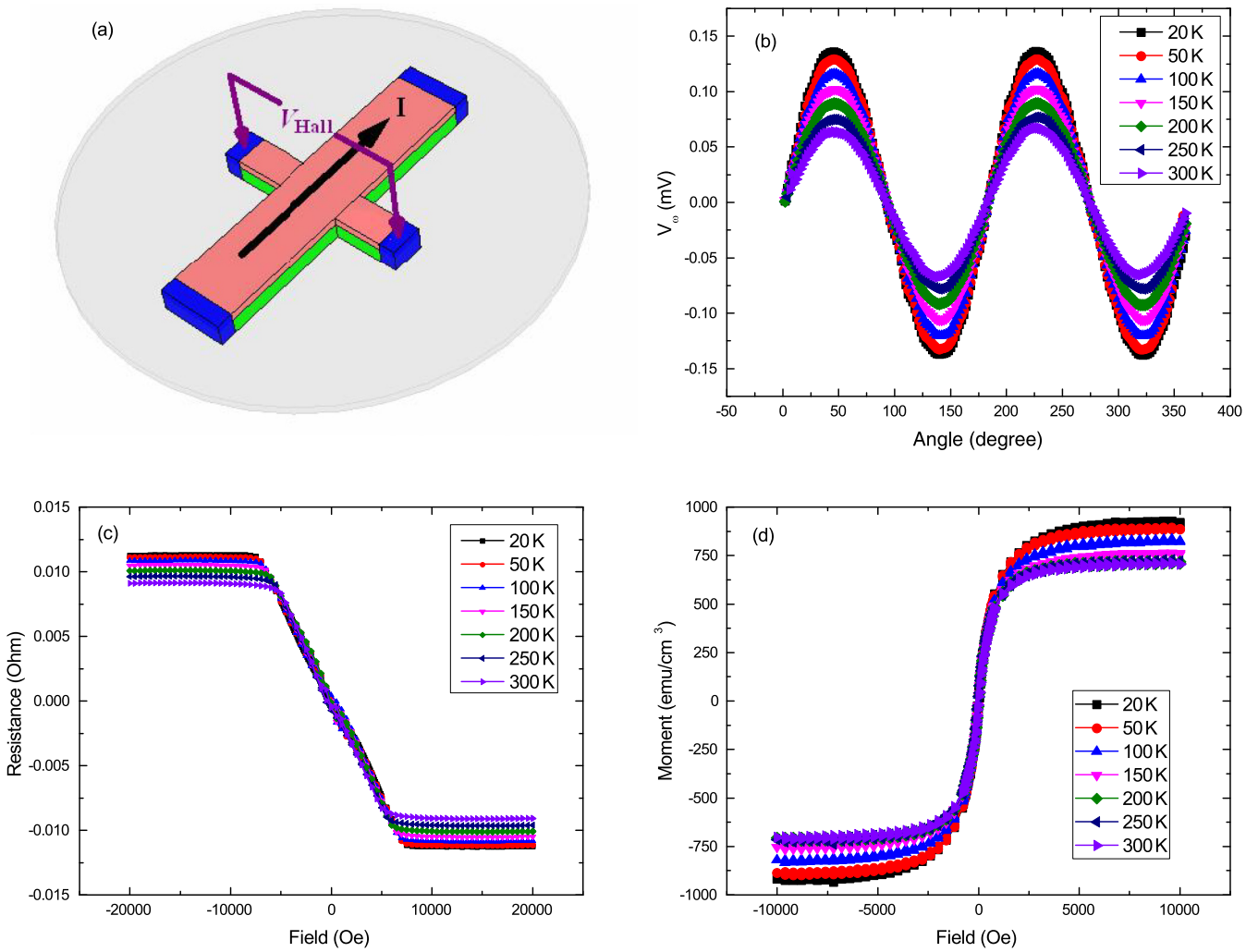

FIG. 1. (a) Schematic of the measurement geometry. (b) The first harmonic voltage V_ω as a function of the azimuthal angle φ (PHE) at different temperatures. (c) Anomalous Hall resistance as a function of the external field measured at various temperatures. (d) The magnetization curves of NiFe (1.5) as a function of temperature.

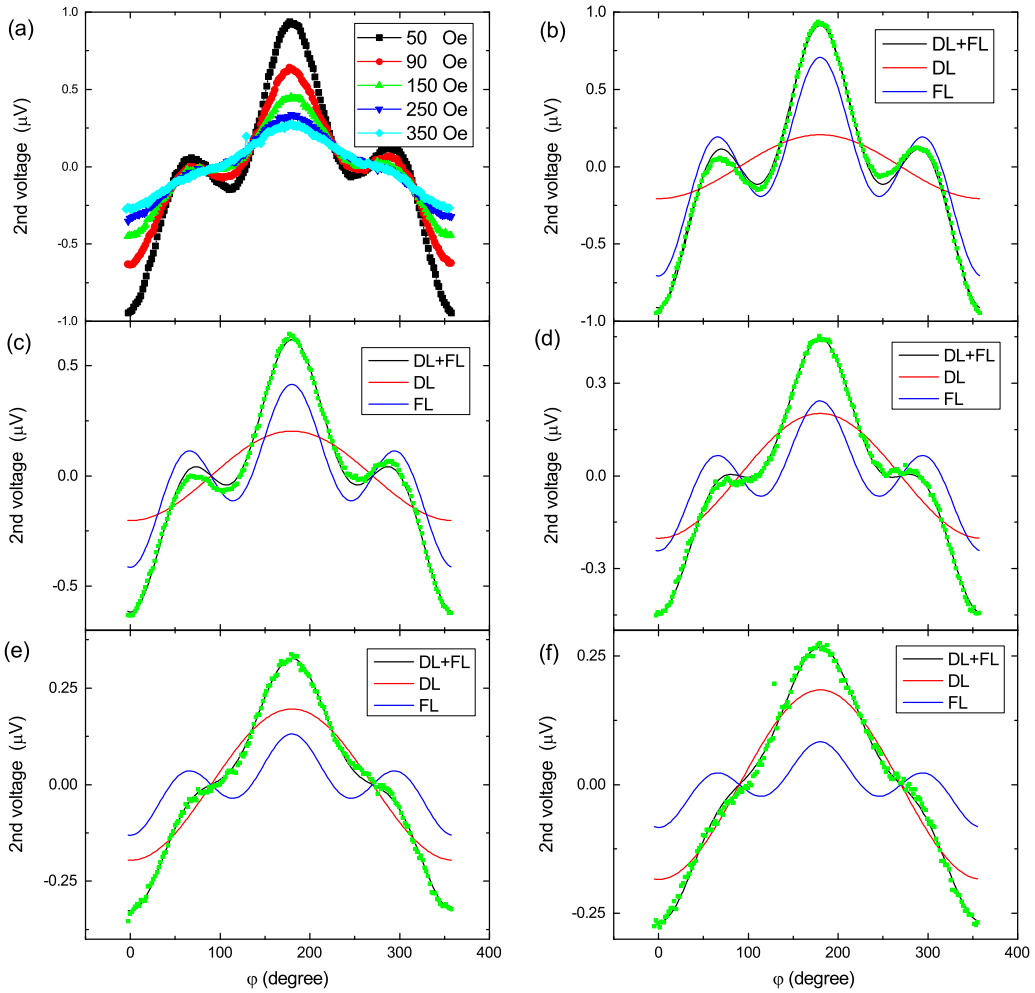

FIG. 2. (a) Second harmonic voltage $V_{2\omega}$, as a function of the azimuthal angle φ, measured at 300 K. (b)–(f) Fitting by Eq. (2) from 50 to 350 Oe. The red line is the $\cos\varphi$ term, i.e., the dampinglike torque. The blue line is the $2\cos^3\varphi - \cos\varphi$ term, i.e., the fieldlike torque.

external field even at 50 Oe, i.e., anisotropy field $|H_A| < 50$ Oe. Close analysis reveals that $|H_A| \sim 10$ Oe. A slight shape deviation and a decrease in R_P with increasing temperature are observed at this field. The dependence of Hall resistance on perpendicular external fields obtained at different temperatures is shown in Fig. 1(c). The nearly linear dependence of Hall effect on the magnetic field and the very small coercive field (<50 Oe) indicate clearly that the magnetization is lying in the film plane, and the perpendicular magnetic anisotropy is very weak. In this case, the Hall effect will saturate at the magnetic fields being equal to the demagnetization fields at different temperatures. The demagnetizing field varies from about 5 to 7 kOe, as the temperature deceases from 300 to 20 K, which is ascribed to the temperature dependent saturation magnetization. To gain a deeper understanding of the magnetic properties of the bilayers, we carefully studied the magnetization as a function of temperature and field. Figure 1(d) shows the in-plane magnetization versus magnetic field curves (up to ± 1 T), measured at various temperatures between 20 and 300 K. A magnetic field of 0.5 T is required to saturate the magnetization, as M_s decreases linearly with temperature, rather than following Bloch's $T^{3/2}$ law due to the two dimensional nature of the samples. The temperature dependence of saturation magnetization $M_s(T)$ is useful in understanding the dependence of the spin Hall angle on temperature.

The second harmonic voltage $V_{2\omega}$, as a function of the azimuthal angle, φ, measured at 300 K, is shown in Fig. 2(a), which is obtained by rotating the sample in the xy plane with a fixed external field; $V_{2\omega}$ exhibits a strong dependence on the field: as the applied field increases, the amplitude of $V_{2\omega}$ weakens. For example, at a low field (50 Oe), a shoulderlike shape around $\varphi = 90°, 270°$ is evident, whereas, at a relatively high field (350 Oe), $V_{2\omega}$ becomes dependent on $\cos\varphi$ in addition to the reduced amplitude. By fitting Eq. (3) to the experimental data, we can separate the second harmonic signal into the dampinglike and fieldlike contributions, as shown in Figs. 2(b)–2(f). The black line is the sum of both dampinglike and fieldlike terms that matches the experimental data (the green dots) well. The red and blue lines represent the dampinglike and fieldlike contributions, respectively. The dampinglike contributions have $\cos\varphi$ dependence, and their amplitudes are all about 0.2 μV at five different fields. The fieldlike contribution decreases with increasing external field, which is in agreement with the prediction of Eq. (3).

The PHE measurements showed that magnetization is saturated in-plane at any of the measured fields and that the

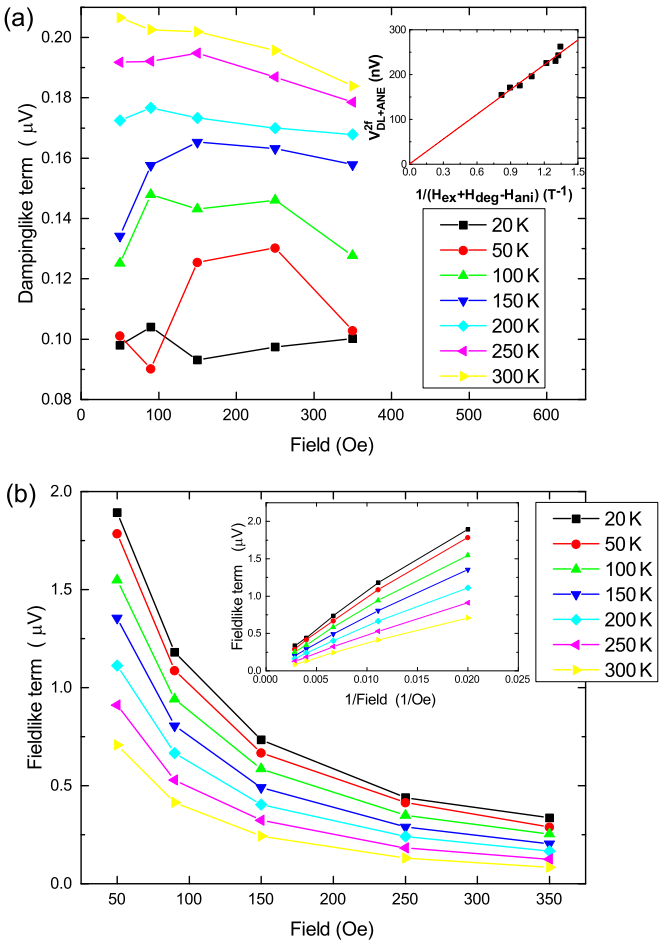

FIG. 3. External field dependence of the extracted (a) dampinglike term at different temperatures (inset: $1/H_{\rm eff}$ dependence measured at 300 K from 250 to 5000 Oe.) and (b) fieldlike term (inset: $1/H$ dependence).

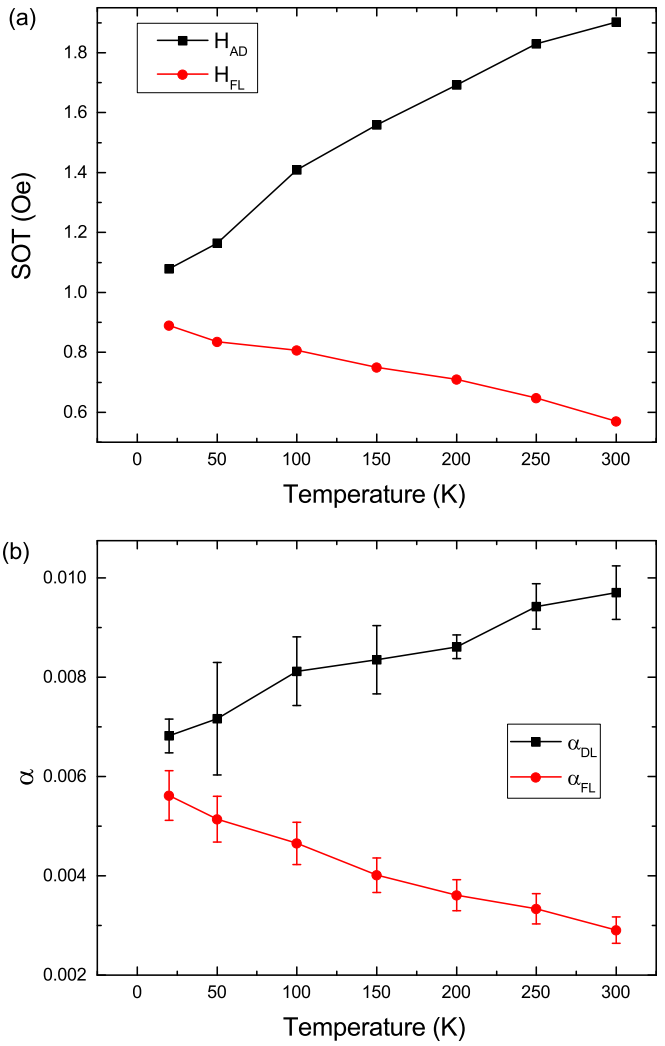

FIG. 4. (a) Temperature dependence of the effective field induced by dampinglike torque and fieldlike torque. (b) Temperature dependence of the electrical efficiency defined as $\alpha_{\rm DL,FL} = \frac{H_{\rm DL,FL}}{J_c}\frac{M_s t_{\rm FM}}{\hbar/2e}$.

PHE coefficient R_P is independent of the external field. Hence, the fieldlike torque is inversely proportional to the external field. Figure 3(b) shows the fieldlike term in relation to the external field obtained at different temperatures. The external field is much smaller than the demagnetization field, which is obtained from the AHE measurements. It, thus, follows that as suggested by Eq. (3), the dampinglike torque is independent of the external field, as shown in Fig. 3(a). We note, however, that the result measured at 50 K is unexpected. We take the average of the values obtained at five different external fields to be the dampinglike torque. To measure the thermal contribution to the SOTs, we extracted the dampinglike torque also at high fields, which is shown in the inset of Fig. 3(a). From Eq. (3), we know the dampinglike torque should vanish at high field. Hence, the intercept corresponds to infinitely large field at which no dampinglike torque should contribute to the second harmonic voltage. Therefore, the intercept should reflect the anomalous Nernst effect (ANE) contribution. The linear relation between them and a near zero intercept, shown in Fig. 3(a), indicate clearly that the thermoelectric effect is very small here.

We depict SOTs (fieldlike and dampinglike torque obtained separated through fitting) as a function of temperature in Fig. 4(a). Although both types of torque exhibit nearly linear dependence on temperature, they follow opposite trends, i.e., the dampinglike torque increases with increasing temperature, whereas the fieldlike torque decreases with increasing temperature. Using the equation

$$\alpha_{\rm DL,FL} = \frac{\tau_{\rm DL,FL}}{J_c}\frac{M_s t_{\rm FM}}{\hbar/2e}, \tag{4}$$

we calculated the electrical efficiency [26] for 8 nm Cu Au alloy, as shown in Fig. 4(b), $\alpha_{\rm DL}$ increases from 0.0068 at 20 K to 0.0097 at 300 K. This result is comparable with SHA in Au [27].

To gain a deeper understanding of the dependence of fieldlike and dampinglike torque on temperature and to explore the origin of these two types of torque further, we studied two additional samples with different NM layer thicknesses. To avoid the difference in current density caused by resistivity and thickness, we converted the current density to 10^8A/cm^2. We found that the thicker the NM layer, the larger the SOTs. According to drift diffusion theory [25], the spin current induced from the bulk SHE is $J_s(t_N)/J_s(\infty) = 1 - \mathrm{sech}(t_N/\lambda_{sf})$,

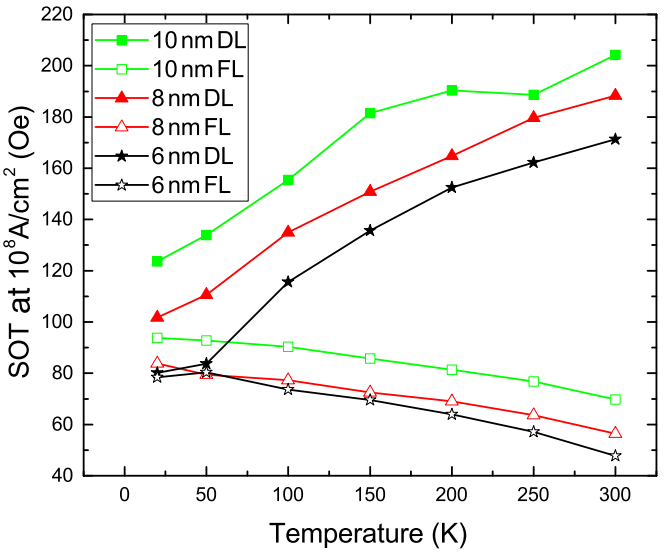

FIG. 5. Thickness dependence of the effective field induced by dampinglike torque and fieldlike torque. The filled and unfilled symbols indicate dampinglike and fieldlike torque, respectively. All current densities are converted to 10^8 A/cm^2.

where t_N is the thickness of the NM layer and λ_{sf} is the spin diffusion length in the NM layer. Based on this relation, the spin current increases with the thickness of the NM layer and saturates only when this thickness reaches the order of the spin diffusion length. Since the spin diffusion length is around several hundreds of nanometers in copper and several tens of nanometers in Au [27,28], the spin diffusion length in CuAu alloy may have the same order of thickness as the NM layer in our samples. A previous study reported the spin diffusion length in CuAu to be ∼5 nm [27], which means that the spin current increases but does not saturate within the range of the sample thickness. In Fig. 5, we plot SOTs as a function of temperature for samples with different NM layer thickness. The bulk SHE remains the main source for dampinglike torque given the strong thickness dependence. Qiu *et al.* [21] and Kim *et al.* [22] observed in Ta/CoFeB/MgO stacks that the fieldlike torque decreased linearly with decreasing temperature, while the dampinglike torque remained mostly unaffected. These observations differ from our observations, likely because in a metal with strong spin-orbit coupling, such as Ta and Pt, intrinsic SHE is the dominant source of SOTs, whereas in our CuAu samples, extrinsic SHE is the dominant mechanism. With increasing temperature and thereby increasing scattering events, intrinsic SHE is not significantly affected and extrinsic SHE increases linearly. Thus, a different dependence on temperature should be expected. The effective field of the dampinglike torque linearly increased from ∼80−120 Oe at 20 K to ∼170−210 Oe at 300 K. In three samples with different NM layer thicknesses, the dampinglike torque increased by about 90 Oe, as the temperature varied from 20 to 300 K. Meanwhile, the fieldlike torque decreased from ∼80−100 Oe at 20 K to ∼50−70 Oe at 300 K.

Theoretically, anomalous Hall resistivity in FM materials should scale quadratically or linearly with longitudinal resistivity (ρ) [29]. The quadratic dependence is posited to come from the extrinsic side jump or intrinsic mechanism, whereas the linear one originated from skew scattering. The typically weak dependence of the metallic resistivity on temperature is presented in Fig. 6(a). Less than 10% variation in the resistivity, ranging from 26.5 $\mu\Omega$ cm at 20 K to 29.0 $\mu\Omega$ cm at 300 K, is evident. Temperature dependent phonon electron scattering is, thus, not the main source of the change in longitudinal resistivity. Instead, scattering caused by structural disorders in the CuAu layer may play the dominant role. Figure 6(b) shows the relation [6] between α_{DL} and resistivity in our samples. Linear dependence may be the best description of this relation, suggesting that the skew scattering may be the dominant source for the SHE in these samples.

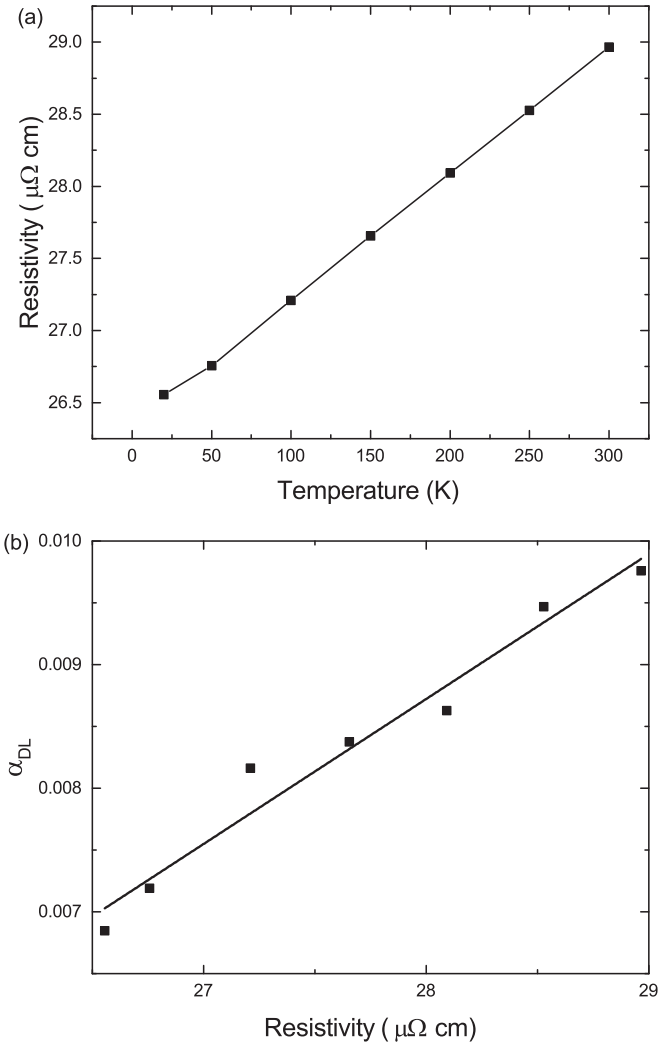

FIG. 6. (a) Resistivity of CuAu (8) as a function of temperature. (b) Relation between α_{DL} and resistivity.

The temperature dependence of the fieldlike torque also deserves some discussion. In Refs. [21,22], it is found that in Ta, the fieldlike torque increased with temperature. Within the scenario of interfacial Rashba torque, this increase in fieldlike torque could be attributed to an increase in bulk resistance upon increase in temperature, thereby increasing the current flowing through the interface. This enhancement can therefore be

accompanied by an increase in fieldlike torque. In contrast, our experiments show that in CuAu, the fieldlike torque decreases when increasing temperature. Although it is difficult to quantitatively interpret this result, we speculate that Rashba spin-orbit coupling is weak at the interface between Au and NiFe [30]. Therefore, in the absence of Rashba spin-orbit coupling, a possible origin of the fieldlike torque can be the presence of spin swapping in CuAu, where extrinsic spin-orbit scattering dominates the transport. Increasing the temperature would then lead to a decrease in fieldlike torque, as suggested by a recent theory [31]. We emphasize that this explanation remains speculative and requires further experiments to be confirmed.

In summary, we used a reliable and convenient method to separate dampinglike torque and fieldlike torque by using experimental data of the harmonic voltage of the transverse resistance. The second harmonic voltage $V_{2\omega}$ contains two components, the fieldlike and dampinglike terms. The dampinglike term has a $\cos\varphi$ dependence, and the fieldlike term has a $2\cos^3\varphi - \cos\varphi$ dependence, which allows us to separate these two contributions by scanning the angle of the in-plane field. This technique is suitable for in-plane magnetized systems, while most previous methods can be used only in systems with out of plane magnetization. This method can also be used for out of plane systems only if the external field is strong enough to overcome the perpendicular anisotropy. Importantly, we found that dampinglike torque and fieldlike torque depend on temperature very differently. With increasing temperature, the dampinglike torque increases, but the fieldlike torque decreases. The temperature behavior of dampinglike and fieldlike torque may, respectively, arise from extrinsic skew scattering and spin swapping in CuAu alloys. We also found larger SOTs (both dampinglike torque and fieldlike torque) in samples with thick NM layers.

ACKNOWLEDGMENTS

The research reported in this publication was supported by King Abdullah University of Science and Technology (KAUST) under Grant No. CRF 2015 2626 CRG4. The work at the University of Delaware was supported by the US National Science Foundation under Division of Materials Research Grant No. 1505192.

APPENDIX

First, no current is flowing through the stack. In this case, there exist only two energies: anisotropy energy and Zeeman energy. The total magnetic energy of this system is, thus,

$$E = -K_{\text{out}}\cos^2\theta - K_{\text{in}}\sin^2\varphi\sin^2\theta - \vec{M}\cdot\vec{H}, \tag{A1}$$

where K_{out} is the effective out of plane anisotropy constant, K_{in} is the effective in-plane anisotropy constant, and θ and φ are the polar and azimuthal angles of the magnetization moment $\vec{M}$. The moment is defined as

$$\vec{M} = M_S\vec{m} = M_S(\cos\varphi_m\sin\theta_m, \sin\varphi_m\sin\theta_m, \cos\theta_m), \tag{A2}$$

where M_S is the saturation magnetization and $\vec{m}$ is the unit vector of the moment. The external field $\vec{H}$ is expressed with its polar and azimuthal angle (θ_H,φ_H), as

$$\vec{H} = H(\cos\varphi_H\sin\theta_H, \sin\varphi_H\sin\theta_H, \cos\theta_H). \tag{A3}$$

By solving $\frac{\partial E}{\partial\theta} = 0, \frac{\partial E}{\partial\varphi} = 0$, we can obtain the equilibrium value of the magnetization angle (θ_M,φ_M).

When a current is applied to the sample as shown in Fig. 1, the current induced field $\Delta\vec{H}$, which includes both the effective field caused by SOT and the Oersted field, moves the moment with a modulation angle $(\Delta\theta,\Delta\varphi)$.

We define $H_K = 2K_{\text{out}}/M_s$ and $H_A = 2K_{\text{in}}/M_s$ as the out of plane and in-plane effective anisotropy field, respectively. If we assume that $|H_A| \ll |H\sin\theta_H|$, then $0 = \frac{\partial E}{\partial\varphi} = -K_{\text{out}}\sin^2\theta_m\sin 2\varphi_m - M_sH\sin\theta_m\sin\theta_H\sin(\varphi_H - \varphi_m)$ will give $\varphi_m = \varphi_H$.

By solving $\frac{\partial}{\partial H_i}(\frac{\partial E}{\partial\theta}) = 0, \frac{\partial}{\partial H_i}(\frac{\partial E}{\partial\varphi}) = 0$ (subscript i denotes the $i = (X,Y,Z)$ component of the vector), we have the values of $\frac{\partial\theta}{\partial H_i}$ and $\frac{\partial\varphi}{\partial H_i}$. We substitute these values, respectively, into $\Delta\theta = \sum_i \frac{\partial\theta}{\partial H_i}\Delta H_i$ and $\Delta\varphi = \sum_i \frac{\partial\varphi}{\partial H_i}\Delta H_i$, which yield

$$\Delta\theta = \frac{\cos\theta_m(\Delta H_X\cos\varphi_H + \Delta H_Y\sin\varphi_H) + \sin\theta_m[C(-\Delta H_X\sin\varphi_H + \Delta H_Y\cos\varphi_H) - \Delta H_Z]}{(H_K - H_A\sin^2\varphi_H)\cos 2\theta_m + H\cos(\theta_H - \theta_m) - \frac{1}{2}CH_A\sin 2\theta_m\sin 2\varphi_H} \tag{A4}$$

$$\Delta\varphi = \frac{([(H_K - H_A\sin^2\varphi_H)\cos 2\theta_0 + H\cos(\theta_H - \theta_0)](-\Delta H_x\sin\varphi_H + \Delta H_Y\cos\varphi_H))}{\left[(H_K - H_A\sin^2\varphi_H)\cos 2\theta_0 + H\cos(\theta_H - \theta_0) - \frac{1}{2}CH_A\sin 2\theta_0\sin 2\varphi_H\right][-H_A\sin\theta_0\cos 2\varphi_H + H\sin\theta_H]}$$
$$+ \frac{H_A\sin 2\varphi_H\left[\cos^2\theta_0(-\Delta H_x\sin\varphi_H + \Delta H_Y\cos\varphi_H) - \frac{1}{2}\sin 2\theta_0\Delta H_Z\right]}{\left[(H_K - H_A\sin^2\varphi_H)\cos 2\theta_0 + H\cos(\theta_H - \theta_0) - \frac{1}{2}CH_A\sin 2\theta_0\sin 2\varphi_H\right][-H_A\sin\theta_0\cos 2\varphi_H + H\sin\theta_H]}, \tag{A5}$$

where $C = \frac{H_A\cos\theta_m\sin 2\varphi_H}{-H_A\sin\theta_m\cos 2\varphi_H + H\sin\theta_H}$ [17].

We now consider the relationship between the Hall resistance and the modulation angle. The Hall resistance typically contains contributions from the PHE and the AHE. Previous reports express the Hall resistance as

$$R_H = R_A\cos\theta + R_P\sin^2\theta\sin 2\varphi, \tag{A6}$$

where R_A and R_P are the coefficient of AHE and PHE, respectively. The current induced field here is small compared with the external field. We can, thus, assume that the modulation angle $\Delta\theta,\Delta\varphi$ is very small. Thus, we can expand Eq. (A6) to

$$R_H = R_A(\cos\theta_m - \Delta\theta\sin\theta_m) + R_P(\sin^2\theta_m + \Delta\theta\sin 2\theta_m) \times(\sin 2\varphi_m + 2\Delta\varphi\cos 2\varphi_m). \tag{A7}$$

It turns out that measuring the in-plane external field ($\theta_H = \pi/2$) is sufficient if samples have large out of plane anisotropy ($|H_K| \gg |\Delta H_Z|$) to maintain an almost in-plane moment ($\theta_m = \pi/2$). Thus, the Hall resistance can be simplified to

$$R_H = R_P \sin 2\varphi_m + (\Delta\varphi \cdot 2R_p \cos 2\varphi_m - \Delta\theta \cdot R_A). \quad \text{(A8)}$$

Simultaneously, the modulation angle can be simplified to

$$\Delta\theta = \frac{\Delta H_Z}{H_K - H}, \quad \text{(A9)}$$

$$\Delta\varphi = \frac{-\Delta H_X \sin\varphi_H + \Delta H_Y \cos\varphi_H}{H - H_A}. \quad \text{(A10)}$$

When an alternating current ($i = I \sin\omega t$) is applied, the current induced field oscillates in the same frequency with the current. We can, thus, replace $\Delta\theta, \Delta\varphi$ with $\Delta\theta \sin\omega t, \Delta\varphi \sin\omega t$. Therefore, the Hall voltage can be expressed as

$$V_H = [R_P \sin 2\varphi_m \sin\omega t + (\Delta\varphi \cdot 2R_p \cos 2\varphi_m - \Delta\theta \cdot R_A) \times \sin^2\omega t]I. \quad \text{(A11)}$$

Here, we separate the Hall voltage into three parts determined by the frequency. The useful parts are the first and second harmonic Hall voltage, since the zero order part can be easily affected by the dc offset of the sinusoidal current:

$$V_H = V_0 + V_\omega \sin\omega t + V_{2\omega} \cos 2\omega t \quad \text{(A12)}$$

$$V_\omega = R_P \sin 2\varphi_m \cdot I$$
$$V_{2\omega} = -V_0 = \left(-\Delta\varphi \cdot R_p \cos 2\varphi_m + \tfrac{1}{2}\Delta\theta \cdot R_A\right)I. \quad \text{(A13)}$$

Using Eq. (A9), Eq. (A10) and $\varphi \equiv \varphi_m = \varphi_H$, we will have

$$V_\omega = R_P \sin 2\varphi \cdot I$$
$$V_{2\omega} = \left(\frac{\Delta H_X \sin\varphi - \Delta H_Y \cos\varphi}{H - H_A} \cdot R_p \cos 2\varphi + \frac{1}{2}\frac{\Delta H_Z}{H_K - H} \cdot R_A\right)I. \quad \text{(A14)}$$

To determine fieldlike torque and antidamping torque quantitatively, we need to use the Landau-Lifshitz-Gilbert equation:

$$\frac{d\vec{m}}{dt} = -\gamma\vec{m} \times [\vec{H} + \alpha(\vec{m} \times \vec{H}) + H_{\mathrm{FL}}\vec{\sigma} + H_{\mathrm{AD}}(\vec{m} \times \vec{\sigma})]. \quad \text{(A15)}$$

Here, γ is the gyromagnetic ratio, α is the Gilbert damping coefficient, $\vec{H}$ is the external field, and $\vec{\sigma}$ is the normalized net spin direction among the electrons absorbed by the FM layer. Also, $\overrightarrow{H_{\mathrm{FL}}} = H_{\mathrm{FL}}\vec{\sigma}$ and $\overrightarrow{H_{\mathrm{DL}}} = H_{\mathrm{DL}}(\vec{m} \times \vec{\sigma})$ are effective fields induced by fieldlike torque and dampinglike torque, respectively. Here, for the in-plane scan, we have $\vec{m} = (\cos\varphi, \sin\varphi, 0)$ and $\vec{\sigma} = (0,1,0)$, which leads to $\overrightarrow{H_{\mathrm{FL}}} = (0, H_{\mathrm{FL}}, 0)$ and $\overrightarrow{H_{\mathrm{DL}}} = (0, 0, H_{\mathrm{DL}} \cos\varphi)$. Substituting into Eq. (A14), we have

$$V_{2\omega} = \left(\frac{-H_{\mathrm{FL}} \cos\varphi}{H - H_A} \cdot R_p \cos 2\varphi + \frac{1}{2}\frac{H_{\mathrm{DL}} \cos\varphi}{H_K - H} \cdot R_A\right)I. \quad \text{(A16)}$$

The second harmonic voltage now can be separated by $\cos\varphi$ and $2\cos^3\varphi - \cos\varphi$ dependence, which corresponds to dampinglike torque and fieldlike torque.

[1] T. Jungwirth, J. Wunderlich, and K. Olejnik, Nat. Mater. **11**, 382 (2012).
[2] A. Brataas, A. D. Kent, and H. Ohno, Nat. Mater. **11**, 372 (2012).
[3] F. Matsukura, Y. Tokura, and H. Ohno, Nat. Nanotechnol. **10**, 209 (2015).
[4] P. Gambardella and I. M. Miron, Philos. Trans. R. Soc. A **369**, 3175 (2011).
[5] A. Manchon, H. C. Koo, J. Nitta, S. M. Frolov, and R. A. Duine, Nat. Mater. **14**, 871 (2015).
[6] Q. Hao and G. Xiao, Phys. Rev. B **91**, 224413 (2015).
[7] L. Liu, C. F. Pai, Y. Li, H. W. Tseng, D. C. Ralph, and R. A. Buhrman, Science **336**, 555 (2012).
[8] S. O. Valenzuela and M. Tinkham, Nature (London) **442**, 176 (2006).
[9] I. M. Miron, K. Garello, G. Gaudin, P. J. Zermatten, M. V. Costache, S. Auffret, S. Bandiera, B. Rodmacq, A. Schuhl, and P. Gambardella, Nature (London) **476**, 189 (2011).
[10] P. M. Haney, H. W. Lee, K. J. Lee, A. Manchon, and M. D. Stiles, Phys. Rev. B **87**, 174411 (2013).
[11] H. B. M. Saidaoui, Y. Otani, and A. Manchon, Phys. Rev. B **92**, 024417 (2015).
[12] U. H. Pi, K. W. Kim, J. Y. Bae, S. C. Lee, Y. J. Cho, K. S. Kim, and S. Seo, Appl. Phys. Lett. **97**, 162507 (2010).
[13] J. Kim, J. Sinha, M. Hayashi, M. Yamanouchi, S. Fukami, T. Suzuki, S. Mitani, and H. Ohno, Nat. Mater. **12**, 240 (2013).
[14] K. Garello, I. M. Miron, C. O. Avci, F. Freimuth, Y. Mokrousov, S. Blugel, S. Auffret, O. Boulle, G. Gaudin, and P. Gambardella, Nat. Nanotechnol. **8**, 587 (2013).
[15] C. O. Avci, K. Garello, M. Gabureac, A. Ghosh, A. Fuhrer, S. F. Alvarado, and P. Gambardella, Phys. Rev. B **90**, 224427 (2014).
[16] C. O. Avci, K. Garello, C. Nistor, S. Godey, B. Ballesteros, A. Mugarza, A. Barla, M. Valvidares, E. Pellegrin, A. Ghosh, I. M. Miron, O. Boulle, S. Auffret, G. Gaudin, and P. Gambardella, Phys. Rev. B **89**, 214419 (2014).
[17] M. Hayashi, J. Kim, M. Yamanouchi, and H. Ohno, Phys. Rev. B **89**, 144425 (2014).
[18] M. Jamali, K. Narayanapillai, X. Qiu, L. M. Loong, A. Manchon, and H. Yang, Phys. Rev. Lett. **111**, 246602 (2013).
[19] X. Fan, J. Wu, Y. Chen, M. J. Jerry, H. Zhang, and J. Q. Xiao, Nat. Commun. **4**, 1799 (2013).
[20] X. Fan, H. Celik, J. Wu, C. Ni, K. J. Lee, V. O. Lorenz, and J. Q. Xiao, Nat. Commun. **5**, 3042 (2014).

[21] X. Qiu, P. Deorani, K. Narayanapillai, K. S. Lee, K. J. Lee, H. W. Lee, and H. Yang, Sci. Rep. **4**, 4491 (2014).
[22] J. Kim, J. Sinha, S. Mitani, M. Hayashi, S. Takahashi, S. Maekawa, M. Yamanouchi, and H. Ohno, Phys. Rev. B **89**, 174424 (2014).
[23] M. Morota, Y. Niimi, K. Ohnishi, D. H. Wei, T. Tanaka, H. Kontani, T. Kimura, and Y. Otani, Phys. Rev. B **83**, 174405 (2011).
[24] T. Tanaka, H. Kontani, M. Naito, T. Naito, D. S. Hirashima, K. Yamada, and J. Inoue, Phys. Rev. B **77**, 165117 (2008).
[25] L. Liu, T. Moriyama, D. C. Ralph, and R. A. Buhrman, Phys. Rev. Lett. **106**, 036601 (2011).
[26] H. Li and A. Manchon, Phys. Rev. B **93**, 235317 (2016).
[27] J. Wu, L. Zou, T. Wang, Y. Chen, J. Cai, J. Hu, and J. Xiao, IEEE Trans. Magn. **52**, 4100204 (2016).
[28] M. Isasa, E. Villamor, L. E. Hueso, M. Gradhand, and F. Casanova, Phys. Rev. B **91**, 024402 (2015).
[29] N. Nagaosa, J. Sinova, S. Onoda, A. H. MacDonald, and N. P. Ong, Rev. Mod. Phys. **82**, 1539 (2010).
[30] S. Grytsyuk, A. Belabbes, P. M. Haney, H.-W. Lee, K.-J. Lee, M. D. Stiles, U. Schwingenschlögl, and A. Manchon, Phys. Rev. B **93**, 174421 (2016).
[31] H. B. M. Saidaoui and A. Manchon, Phys. Rev. Lett. **117**, 036601 (2016).